J. Phys. B: At. Mol. Opt. Phys. **33** (2000) 1687–1702. Printed in the UK PII: S0953-4075(00)09375-5

Electron scattering from N_2O: absolute elastic scattering and vibrational excitation

M Kitajima†, Y Sakamoto†, R J Gulley‡, M Hoshino†, J C Gibson‡, H Tanaka† and S J Buckman‡

† Department of Physics, Sophia University, Tokyo 102-8554, Japan
‡ Research School of Physical Sciences and Engineering, Australian National University, Canberra, Australia

Received 8 November 1999, in final form 18 February 2000

Abstract. We report absolute measurements, using the relative flow technique, of low-to-intermediate energy (1.5–100 eV) differential cross sections (DCSs) for elastic electron scattering and vibrational excitation of nitrous oxide. These results, which have been undertaken independently in our two laboratories on different experimental apparatus, are compared in detail with each other and with previous experimental results and theoretical calculations. For elastic scattering the level of agreement between the DCSs from the two laboratories is generally very good. However, the agreement with recent theoretical calculations is rather poor, particularly at energies below 10 eV. For vibrational excitation DCS results have been measured at 2.4 and 8 eV—energies corresponding to the positions of two broad $^2\Pi$ and $^2\Sigma$ shape resonances respectively.

1. Introduction

Nitrous oxide (N_2O) is one of the simplest, stable, linear triatomic molecules and as such it has been the subject of a reasonable amount of study in recent years from both an experimental and a theoretical perspective. It is an important molecule for the chemistry of our own upper atmosphere (for example, it plays a role in the destruction of the ozone layer), it has important applications in medicine, including its use in lasers and as a well known anaesthetic, and it is used in several technological processes involving cold plasmas. It is also one of the first triatomic molecules to which the recently developed polyatomic *R*-matrix scattering code has been applied (Sarpal *et al* 1996, Morgan *et al* 1997). Recently, there have been several other theoretical approaches using the Schwinger multichannel technique (Michelin *et al* 1996, da Costa and Bettega 1998, Winstead and McKoy 1998).

Experimental measurements of differential electron scattering from N_2O date back to the early 1980s (Kubo *et al* 1981, Marinkovic *et al* 1986) and during the 1990s several new measurements at lower energies were undertaken (Johnstone and Newell 1993), including some of the present work which has been reported previously (Kitajima *et al* 1999). There have also been a number of measurements of the total scattering cross section using electron beam attenuation techniques (Zecca *et al* 1974, Szmytkowski *et al* 1984, Kwan *et al* 1984).

The main objectives of the present collaborative work were:

(a) to investigate, in detail, the level of quantitative agreement between the results for absolute elastic electron scattering from the two spectrometers used for the measurements, one at Sophia University (SU) and one at the Australian National University (ANU);

0953-4075/00/091687+16$30.00

(b) to provide the first measurements of absolute vibrational differential cross sections (DCS) for N_2O at a number of low incident energies;
(c) to critically evaluate the level of agreement between experiment and contemporary scattering theory, particularly for low incident energies;
(d) to provide a set of integral cross sections for this molecule which can be compared with and contrasted to measurements of the total scattering cross section.

2. Experimental apparatus and techniques

Both sets of experimental apparatus that have been used in these measurements have been described in detail in previous communications (SU—Tanaka *et al* 1988; ANU—Gulley *et al* 1994, Gibson *et al* 1999) and will not be repeated here in detail. Rather, each apparatus will be described briefly and we shall attempt to highlight and discuss a number of similarities and differences between the apparatus and techniques used in each laboratory.

In both scattering apparatus, hemispherical electron monochromators and energy analysers are used for electron beam production and analysis, in conjunction with electrostatic electron optical elements. Whilst there are minor differences in design and practice, the overall operation of the two spectrometers is very similar, with both capable of producing low-energy electron beams with an energy width of between 35 and 60 meV and electron beam currents of between 1 and 5 nA. The SU spectrometer employs cylinder electron lenses throughout whilst the ANU apparatus is a mix of cylinder and aperture lenses. Also, Herzog correcting electrodes are used in the SU hemispherical analysers, whilst in the ANU apparatus fringe-field correcting hoops are used to account for the mismatch of the hemispherical field and the cylindrical electron optical elements. Both apparatus are extensively shielded from stray electric and magnetic fields and both use single-channel electron multiplier detectors, standard pulse handling electronics and multichannel scaling techniques for data acquisition.

In both laboratories, the relative flow technique (Srivastava *et al* 1975) is the method of choice for applying an absolute scale to the relative measurements of the elastic angular distributions. Whilst the standard prescription for the application of this technique is reasonably well understood (see, for example, Srivastava *et al* 1975, Nickel *et al* 1989, Buckman *et al* 1993, Sagara and Boesten 1998) there are still many variations that are possible in its application. The technique involves the measurement of relative elastic electron scattering intensities for the gas under study and for a so-called 'standard' gas for which the scattering cross section is well known. In both our laboratories the standard gas that is routinely employed is helium, as it is widely accepted that the elastic differential scattering cross sections for this gas are now very well known at incident energies below 50 eV (e.g. Nesbet 1979, Boesten and Tanaka 1992, Fursa and Bray 1995).

The central requirement for the correct application of this technique is that the experimental conditions must be identical for both of the gases used. In particular, the size of the electron beam must remain constant during measurements with both gases and the sizes of each of the atomic or molecular beams must also be the same. The first condition is relatively easy to fulfil whilst the latter usually requires some careful experimental consideration. Typically, the atomic or molecular beams can vary in size as a result of collisions with the walls of the device that is used to form the beam (e.g. a capillary tube or multicapillary array), or as a result of intra-beam molecular collisions, particularly near the exit of the beam-forming device. Such effects can only really be correctly accounted for by working under conditions of true molecular flow, where the driving pressure of each gas is such that the mean free path of the gas is much greater than the largest dimension of the beam-forming device. In this case the physical dimensions

of the capillary solely determine the molecular beam profile. However, under such conditions, the resulting gas beam densities are so low that scattering experiments with high-resolution electron beams ($I \sim 1$ nA) and gas targets which typically have cross sections of ~ 1 Å^2 are not generally feasible due to low counting rates. As a result a compromise is usually made for the driving pressure that is used. At SU we use a single capillary tube with a diameter $d = 0.3$ mm and length $L = 5$ mm. The driving pressures for helium and N_2O are 6 and 1.5 Torr respectively, based on the requirement that the mean free paths for the two gases are equivalent and that the flow conditions remain in the so-called Clausing regime where the Knudsen number is $K = \lambda/L \leqslant 10$. This criterion has been discussed in several other papers (e.g. Nickel *et al* 1989). At the ANU the beam-forming device is a multicapillary array with individual capillary tubes which are 40 μm in diameter and 1 mm long. As a general 'rule-of-thumb' we require that the mean free path of each gas is greater than twice the tube diameter (i.e. $\lambda > 80$ μm—see Buckman *et al* (1993)) and this results in a maximum driving pressure of 1.2 Torr for helium. This value is based on gas-kinetic calculations using a hard sphere diameter of 2.19 Å for helium. The corresponding hard sphere diameter for N_2O is 4.68 Å (Landölt-Bornstein) resulting in a maximum driving pressure for N_2O of 0.26 Torr if the mean free paths for each gas are matched. We note, however, that the literature contains values of the hard sphere diameter for N_2O which vary from 4.68 to 7.5 Å. This range implies driving pressure ratios for He/N_2O which vary between about 6 and 12. At the ANU we have investigated the dependence of the elastic scattering cross section on this ratio and found no significant effect for absolute pressures below about 1.5 Torr. The gas driving pressure conditions that are used in each laboratory represent perhaps the biggest differences in the two techniques and we shall see that it apparently has little effect on the cross sections that are obtained.

The methods used for data accumulation and application of the relative flow technique are slightly different in each of our laboratories. At SU, a cross section measurement cycle consists of the sequential measurement of the complete angular distribution for each gas and for the background. The scattered electron intensity is measured by scanning the energy-loss voltage of the spectrometer across the elastic (or inelastic) peak and integrating the scattered signal using a multichannel analyser. In each case the electron beam current and gas pressure are carefully monitored and the relative flow technique is then applied point-by-point to obtain the absolute cross section for the target gas. Differential pumping of the monochromator and analyser regions ensures long-term stability of the electron beam current and detection efficiency. At the ANU, the measurements are carried out point-by-point, with the scattered electron intensity determined sequentially for each gas, and the background, at each scattering angle. The system is not differentially pumped but each gas is present in the scattering chamber at all times. The advantages of this technique have been pointed out in a number of recent papers (e.g. Shi *et al* 1993, Buckman *et al* 1994). It helps to maintain stability and avoid contact potential variations with gas cycling. Thus, each measurement cycle consists of three scattering experiments: one with N_2O flowing through the capillary array and helium through a needle located on the vacuum chamber periphery, one with these two gas flows reversed, and one with both gases flowing into the chamber via the peripheral needle to provide the 'background' measurement. Background scattering intensities were normally quite small—less than 10% of the 'signal' levels. The scattered intensities are determined in a similar manner to the SU measurements by integrating over the elastic peak in the energy-loss spectrum. In each experiment, the position of the He^- $1s2s^2$ resonance (Brunt *et al* 1977) or the quasi-vibrational resonance structure in N_2 (Rohr 1977) is used to calibrate the incident electron beam energy. Also, in each experiment, computer control is used for the automation of data accumulation and the continuous monitoring of experimental parameters.

The vibrational excitation cross sections, measured at SU, are derived from measurements of energy-loss spectra. As the energy resolution of the apparatus (∼30 meV) is not sufficient to fully resolve the low-lying vibrational features, each spectrum has been fitted with a series of Gaussian functions centred at the excitation energies of the vibrational modes (010: 073 eV, 100: 0.159 eV, 001: 0.276 eV, 110: 0.232 eV, 200: 0.320 eV). The width of each Gaussian is given by the instrumental resolution function. The area under each of these Gaussians is proportional to the DCS for that state and the absolute value of the cross section is obtained by normalizing to the value for the elastic peak. This procedure has been described in greater detail in a previous paper (Dillon *et al* 1993).

3. Results and discussion

3.1. Elastic scattering

The DCS for elastic scattering are presented in table 1. At each energy there is an indication at the top of each column as to the source of the results—SU or ANU. The SU results are presented for 19 energies between 1.5 and 100 eV and the ANU results for 13 energies between 2.0 and 20 eV. The absolute uncertainty in the DCS from SU are estimated to be no greater than 15% whilst for the ANU results the uncertainty is typically less than 10%.

The results are also presented and compared graphically with previous measurements and calculations in figures 1 and 2. For the sake of brevity we do not present all the data graphically but have chosen representative examples, which both highlight important aspects of the cross sections and demonstrate the level of accord between the two experimental approaches. Figure 1(*a*) shows the cross section at an energy of around 2.3 eV, the position of the low-energy $^2\Pi$ shape resonance. Although the two experimental DCS have been measured at slightly different energies one can still see that the level of agreement is reasonably good—generally within the combined experimental uncertainties. The Schwinger variational calculations of Winstead and McKoy (at an energy of 2.2 eV), which include both exchange and polarization effects, show the same general shape as the experimental DCS. In particular the p-wave behaviour which is expected for the resonance decay is clear; however, the calculated cross sections are considerably larger than experiment at forward and backward angles. This is possibly a result of these calculations being carried out in the fixed nuclei approximation which generally results in resonance effects that are too narrow in energy and too large in magnitude. At 3.0 eV (figure 1(*b*)) the shape of the DCS has already changed from that at the resonance peak (2.3 eV) with the minimum moving to an angle of about 120° and the cross section also beginning to 'turn over' or decrease at forward angles. The agreement between the two experimental DCSs is excellent at all scattering angles. The cross section at 5.0 eV (figure 1(*c*)) has developed a relatively deep minimum at small scattering angles (∼20°) and a secondary maximum between 50° and 60°. The second minimum appears to have moved to an even higher angle and cannot be observed in the present measurements that extend to an angle of 130°. The present experimental results are once again in good agreement with each other but both lie a little lower in magnitude (20–30%) than the previous results of Johnstone and Newell (1993). However, all three experimental DCS show excellent agreement in the shape of the cross section. At this energy there are several calculations with which to compare. In general, they all show the same overall trend and all are in reasonable accord with the shape of the experimental DCS at angles above 60°, in particular the *R*-matrix calculation of Morgan *et al* (1997). However, all of the calculated cross sections fail to reproduce the decrease in the cross section at angles below about 60°, and the subsequent increase for angles less than 20°. This quite remarkable trend in the DCS continues at 6.0 eV (figure 1(*d*)) where the minimum

Table 1. Absolute DCS (in units of 10^{-16} cm^2 sr^{-1}) for elastic electron scattering from N_2O. The uncertainty in the SU data is estimated to be 15% whilst the figures in brackets accompanying the ANU data are the estimated uncertainties expressed as a percentage. Q_i is the integral elastic cross section in units of 10^{-16} cm^2.

Angle	Incident energy (eV)							
(deg)	1.5 (SU)	2.0 (SU)	2.0 (ANU)	2.2 (SU)	2.3 (ANU)	2.4 (SU)	2.5 (SU)	3.0 (SU)
20	1.35	2.35		2.38		2.58	2.42	1.63
25					1.911(14)			
30	0.96	1.82	1.620(9)	2.02	1.753(10)	2.47	2.09	1.78
35					1.678(10)			
40	0.67	1.35	1.149(10)	1.49	1.562(10)	1.97	1.87	1.68
45					1.475(10)			
50	0.46	0.96	0.702(9)	1.18	1.385(9)	1.54	1.51	1.68
55					1.224(7)			
60	0.32	0.71	0.624(9)	0.88	1.099(7)	1.19	1.19	1.48
65					0.922(7)			
70	0.30	0.52	0.479(9)	0.66	0.783(7)	0.93	0.86	1.10
75					0.678(7)			
80	0.30	0.45	0.399(8)	0.52	0.580(7)	0.67	0.64	0.82
85					0.531(7)			
90	0.35	0.45	0.406(9)	0.47	0.503(8)	0.51	0.50	0.62
95					0.491(7)			
100	0.46	0.52	0.478(8)	0.49	0.496(7)	0.47	0.45	0.41
105					0.514(7)			
110	0.56	0.59	0.602(9)	0.59	0.542(7)	0.50	0.50	0.33
115					0.601(7)			
120	0.66	0.78	0.692(10)	0.75	0.699(8)	0.60	0.57	0.28
125					0.826(7)			
130	0.76	1.02	0.825(8)	0.96	0.980(7)	0.77	0.79	0.30
Q_i		12.57	10.14	12.21	12.84	12.90		9.98

	3.0 (ANU)	3.5 (SU)	4.0 (SU)	4.0 (ANU)	5.0 (SU)	5.0 (ANU)	6.0 (SU)	6.0 (ANU)
15						0.722(16)		0.877(21)
16								0.770(19)
17								0.578(12)
18								0.515(14)
20		0.98	0.68	0.640(10)	0.57	0.640(8)	0.60	0.610(8)
25				0.783(11)		0.652(8)		0.661(9)
30		1.10	0.84	0.826(8)	0.62	0.763(7)	0.68	0.769(8)
35	1.747(7)			0.895(9)		0.853(7)		0.859(8)
40	1.761(7)	1.22	1.01	0.990(11)	0.80	0.941(9)	0.86	0.935(8)
45	1.711(7)			1.027(10)		1.011(8)		1.000(8)
50	1.663(7)	1.37	1.15	1.038(11)	0.95	1.015(7)	1.02	0.997(7)
55	1.542(7)			1.065(10)		1.029(8)		0.995(8)
60	1.454(7)	1.22	1.10	0.958(8)	1.04	1.041(7)	1.08	0.962(7)
65	1.315(7)			0.925(10)		1.003(7)		0.950(7)
70	1.177(7)	1.08	1.06	0.838(11)	0.94	0.939(8)	0.94	0.869(7)
75	1.041(7)			0.776(10)		0.894(8)		0.840(8)
80	0.906(7)	0.89	0.83	0.714(10)	0.83	0.810(7)	0.77	0.781(7)
85	0.786(7)			0.662(8)		0.754(8)		0.710(7)
90	0.676(7)	0.71	0.70	0.561(11)	0.68	0.666(7)	0.69	0.624(7)
95	0.587(7)			0.501(9)		0.601(7)		0.553(7)

Table 1. (Continued)

Angle	Incident energy (eV)							
(deg)	3.0 (ANU)	3.5 (SU)	4.0 (SU)	4.0 (ANU)	5.0 (SU)	5.0 (ANU)	6.0 (SU)	6.0 (ANU)
100	0.486(7)	0.50	0.58	0.447(10)	0.52	0.502(8)	0.55	0.485(7)
105	0.410(7)			0.373(7)		0.446(7)		0.419(8)
110	0.349(7)	0.39	0.40	0.314(14)	0.40	0.370(8)	0.40	0.368(11)
115	0.307(7)			0.266(8)		0.324(8)		0.317(10)
120	0.280(7)	0.28	0.30	0.245(8)	0.31	0.284(8)	0.30	0.295(10)
125	0.276(7)			0.243(8)		0.260(8)		0.279(11)
130	0.311(8)	0.23	0.25	0.215(9)	0.27	0.249(7)	0.30	0.263(9)
Q_i	11.47		8.34	7.39	7.60	7.96	7.73	8.10

	7.0 (SU)	7.0 (ANU)	7.5 (ANU)	8.0 (SU)	8.0 (ANU)	9.0 (SU)	9.0 (ANU)	10 (SU)
15		0.995(16)	2.224(8)		1.912(15)		3.053(12)	
20	0.94	0.912(7)	1.270(7)	1.62	1.570(7)	2.34	2.382(7)	2.69
25	0.85	0.881(7)	1.063(7)	1.26	1.336(7)		1.860(7)	2.21
30	0.80	0.875(7)	0.977(7)	1.12	1.153(7)	1.53	1.544(7)	1.84
35	0.79	0.916(7)	0.922(7)	0.99	1.067(7)		1.341(7)	1.57
40	0.86	0.945(7)	0.908(7)	0.99	1.043(7)	1.17	1.206(7)	1.34
45	0.93	0.976(7)	0.912(7)	0.99	1.020(7)		1.119(8)	1.19
50	0.99	0.984(7)	0.920(7)	0.95	0.990(7)	1.04	1.028(7)	1.09
55	0.95	0.988(7)	0.908(7)	0.87	0.962(7)		0.956(7)	1.01
60	0.90	0.930(7)	0.861(7)	0.89	0.919(7)	0.86	0.893(7)	0.94
65	0.90	0.887(7)	0.786(8)	0.83	0.864(7)		0.811(9)	0.86
70	0.85	0.849(8)	0.738(7)	0.80	0.806(7)	0.77	0.754(7)	0.78
75	0.83	0.777(7)	0.681(7)	0.74	0.748(7)		0.680(7)	0.74
80	0.74	0.719(7)	0.626(7)	0.70	0.665(7)	0.64	0.610(7)	0.64
85	0.70	0.659(7)	0.568(7)	0.59	0.605(7)		0.550(7)	0.58
90	0.61	0.591(7)	0.508(7)	0.53	0.541(7)	0.51	0.490(7)	0.51
95	0.56	0.518(7)	0.453(7)	0.46	0.482(7)		0.432(7)	0.44
100	0.48	0.454(7)	0.405(7)	0.45	0.424(7)	0.41	0.384(7)	0.40
105	0.39	0.396(7)	0.350(8)	0.39	0.374(7)		0.358(7)	0.36
110	0.36	0.346(7)	0.329(7)	0.36	0.355(7)	0.34	0.356(7)	0.35
115	0.33	0.313(7)	0.305(8)	0.35	0.352(7)		0.377(7)	0.40
120	0.31	0.302(7)	0.322(7)	0.37	0.386(7)	0.43	0.446(7)	0.44
125	0.35	0.324(7)	0.357(8)	0.40	0.462(7)		0.552(7)	0.56
130	0.35	0.369(8)	0.419(7)	0.48	0.653(7)	0.61	0.693(7)	0.69
Q_i		8.34	8.82	9.25	10.35		11.11	10.39

	10 (ANU)	15 (SU)	15 (ANU)	20 (SU)	20 (ANU)	30 (SU)	60 (SU)	100 (SU)
15	4.133(8)		6.454(10)		8.201(8)			
20	3.107(8)	4.38	4.850(7)	6.67	5.661(8)	5.98	4.31	3.23
25	2.566(8)							
30	2.142(8)	2.72	2.869(10)	3.48	2.821(8)	2.60	1.38	0.94
35	1.717(8)							
40	1.517(9)	1.79	1.814(7)	1.88	1.649(8)	1.27	0.63	0.35
45	1.312(8)							
50	1.235(11)	1.29	1.299(8)	1.24	1.099(8)	0.75	0.32	0.19
55	1.122(8)							
60	1.042(11)	0.97	0.987(8)	0.84	0.747(8)	0.45	0.18	0.12
65	0.955(12)							
70	0.878(16)	0.78	0.772(8)	0.61	0.528(8)	0.30	0.11	0.10

Table 1. (Continued)

Angle (deg)	Incident energy (eV)							
	10 (ANU)	15 (SU)	15 (ANU)	20 (SU)	20 (ANU)	30 (SU)	60 (SU)	100 (SU)
75	0.797(12)							
80	0.699(11)	0.59	0.595(8)	0.40	0.345(8)	0.15	0.10	0.09
85	0.626(8)							
90	0.523(11)	0.40	0.396(10)	0.27	0.236(8)	0.16	0.09	0.08
95	0.494(10)		0.336(8)					
100	0.457(12)	0.30	0.293(9)	0.26	0.246(8)	0.23	0.08	0.09
105	0.415(10)		0.278(13)					
110	0.442(13)	0.35	0.339(15)	0.35	0.340(8)	0.27	0.12	0.11
115	0.463(13)							
120	0.525(10)	0.48	0.467(18)	0.52	0.498(9)	0.33	0.19	0.12
125	0.689(15)							
130	0.830(14)	0.72	0.671(9)	0.70	0.696(9)	0.43	0.28	0.14
Q_i	14.36		14.30		13.77		4.27	2.95

at forward angles has become considerably deeper and moved to a smaller angle ($\sim$18°). The good agreement between the two experimental DCS is again observed at this energy, as is the failure of the theoretical calculation, in this case that of da Costa and Bettega (1998), to correctly predict the forward-angle behaviour of the DCS. At energies less than about 10 eV this calculation, which omits the effects of polarization, is generally too large in magnitude.

At 7.0 eV (figure 2(*a*)) the minimum at forward angles has become slightly shallower and moved to a higher scattering angle ($\sim$30–35°). With the exception of the region of this first minimum, where the two experiments differ in magnitude by as much as 20% (the SU DCS being smaller), the two experiments are once again in excellent agreement. It is also interesting to note that the second minimum has reappeared at this energy at an angle of about 120°. The theoretical calculation of da Costa and Bettega shows the same general shape as the experimental DCS at larger angles but predicts the second minimum at a slightly larger angle than either experiment. It once again fails to predict the structure in the DCS at forward angles. At a slightly higher energy of 8.0 eV the DCS has changed shape considerably (figure 2(*b*)). The minimum at forward angles has vanished, developing into a broad shoulder between 30 and 60° which is accompanied by considerably stronger forward scattering at lower angles. The second minimum has moved to a smaller angle ($\sim$110°) and there is good overall agreement between the two present measurements and relatively good agreement with the previous measurement of Johnstone and Newell (1993), although the latter is slightly higher than both of the present DCS at angles between 40° and 120°. Several theoretical calculations are also compared at this energy. The best overall agreement appears to be with the *R*-matrix calculation of Morgan *et al* (1997) which shows the same general shape as the experimental DCSs, despite being a little higher in magnitude at forward angles and lower at backward angles. At 10 eV (figure 2(*c*)—note the log scale), the trend towards strong forward scattering continues and the shoulder has all but disappeared. The second minimum occurs at an angle of $\sim$105°. Here we have compared the present measurements with those of Johnstone and Newell (1993) and Marinkovic *et al* (1986), and the agreement is clearly quite good at all angles. The situation regarding the theoretical calculations is also markedly improved at this energy with most of the DCSs showing a good general agreement with the experiment values. This is particularly true for the CMS calculation of Kitajima *et al* (1999) and the Schwinger calculations of Winstead and McKoy (1998) and da Costa and Bettega (1998).

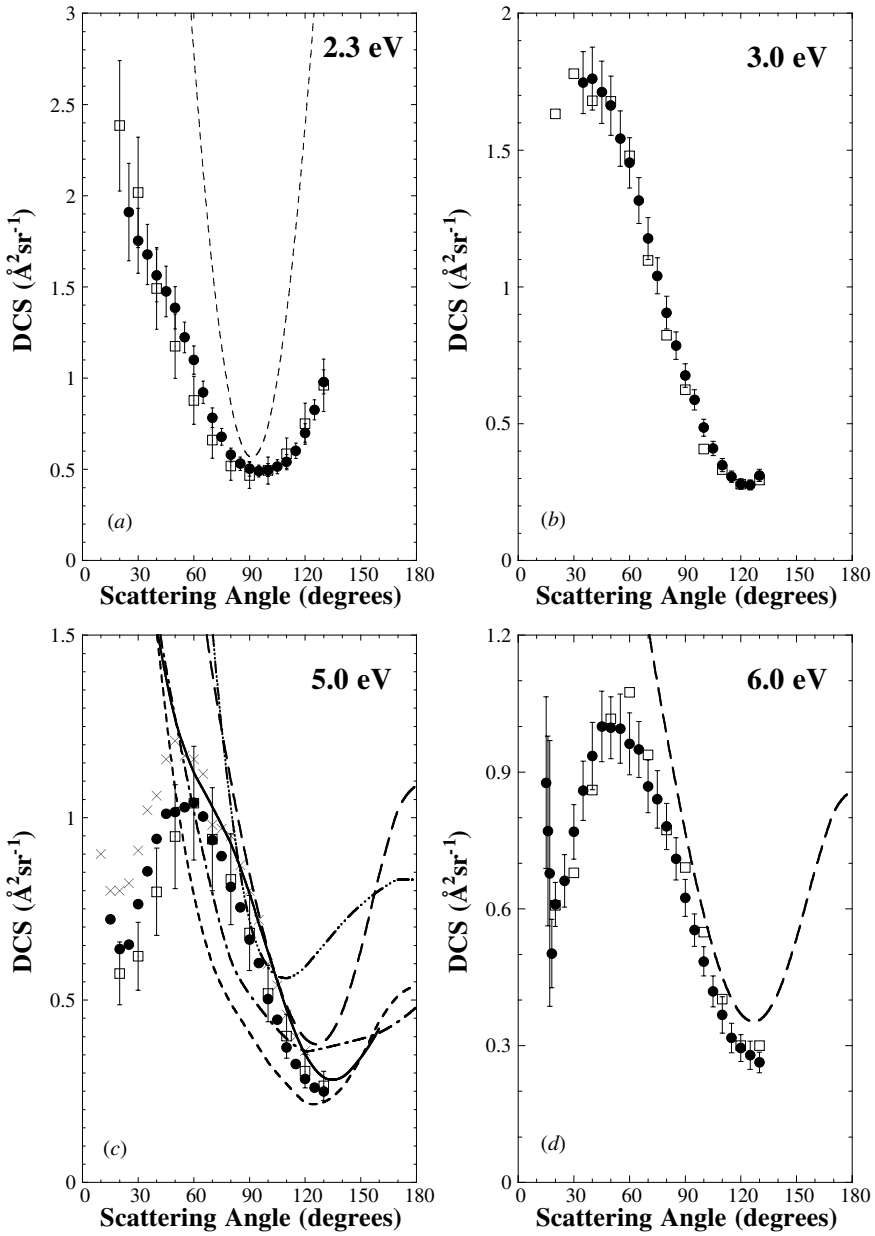

Figure 1. (*a*) Elastic DCS for N_2O at an incident energy near the $^2\Pi$ resonance. (□) Present results, SU, at an energy of 2.2 eV; (●) present results, ANU; (– – –) theory of Winstead and McKoy (1998) at an energy of 2.2 eV. (*b*) Elastic DCS for N_2O at an incident energy of 3.0 eV. (□) Present results, SU; (●) present results, ANU. (*c*) Elastic DCS for N_2O at an incident energy of 5.0 eV. (□) Present results, SU; (●) present results, ANU; (×) Johnstone and Newell (1993); (– – –) theory of Winstead and McKoy (1998); (——) theory of Morgan *et al* (1997); (— — —) theory of da Costa and Bettega (1998); (— · · —) theory of Michelin *et al* (1996); (— · —) theory of Kitajima *et al* (1999). (*d*) Elastic DCS for N_2O at an incident energy of 6.0 eV. (□) Present results, SU; (●) present results, ANU; (— — —) theory of da Costa and Bettega (1998).

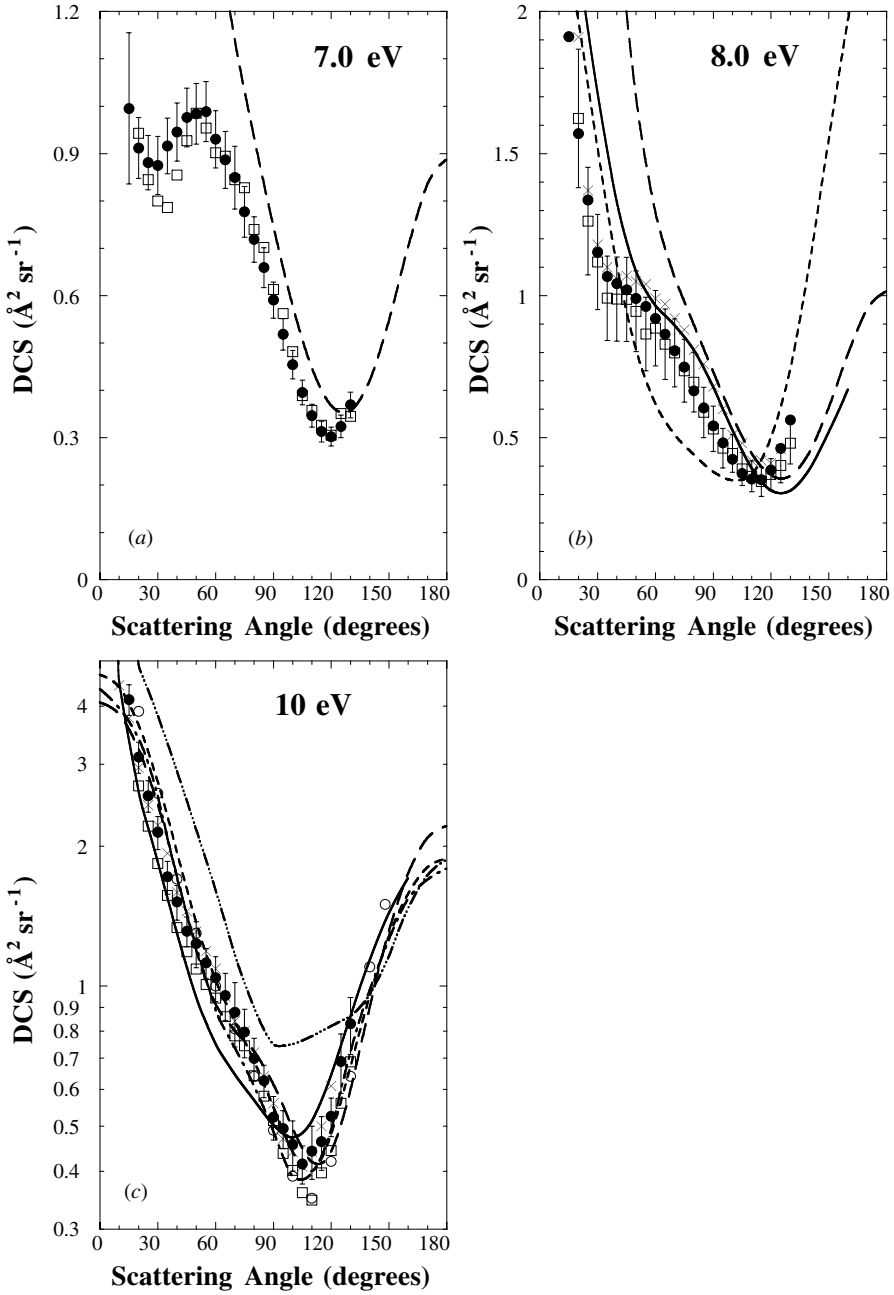

Figure 2. (*a*) Elastic DCS for N_2O at an incident energy of 7.0 eV. (□) Present results, SU; (●) present results, ANU; (— — —) theory of da Costa and Bettega (1998). (*b*) Elastic DCS for N_2O at an incident energy of 8.0 eV. (□) Present results, SU; (●) present results, ANU; (×) Johnstone and Newell (1995); (– – –) theory of Winstead and McKoy (1998); (——) theory of Morgan *et al* (1998); (— — —) theory of da Costa and Bettega (1998). (*c*) Elastic DCS for N_2O at an incident energy of 10 eV. (□) Present results, SU; (●) present results, ANU; (×) Johnstone and Newell (1993); (○) Marinkovic *et al* (1996); (– – –) theory of Winstead and McKoy (1998); (——) theory of Morgan *et al* (1997); (— — —) theory of da Costa and Bettega (1998); (– · · · –) theory of Michelin *et al* (1996); (— · —) theory of Kitajima *et al* (1999).

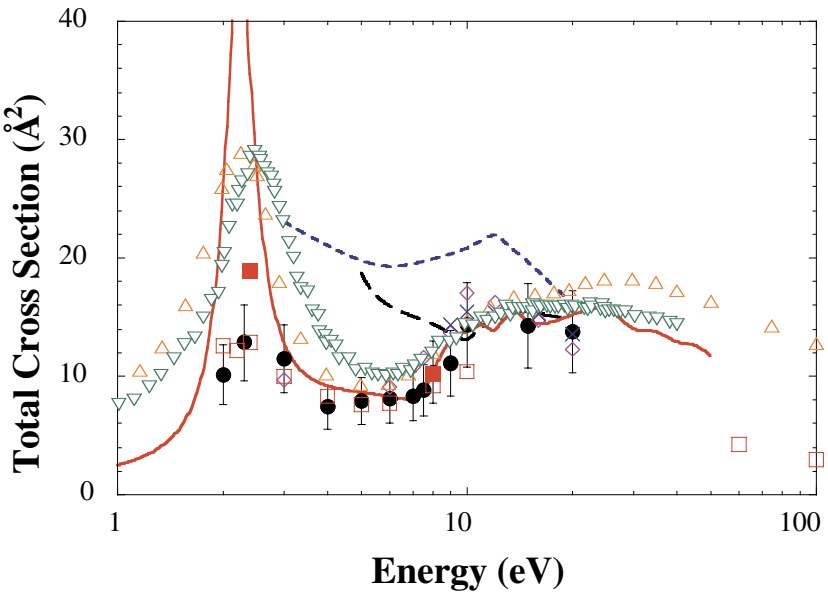

Figure 3. Integral elastic cross section for N_2O at energies up to 100 eV. (●) Present results, ANU; (□) Present data, SU; (◇) Johnstone and Newell (1993); (×) Marinkovic *et al* (1986). Also shown are the grand total cross section data of (△) Kwan *et al* (1984) and (▽) Szmytkowski *et al* (1984) and the theoretical calculations of (– – –) da Costa and Bettega (1998); (——) Winstead and McKoy (1998); (— — —) Michelin *et al* (1996). At 2.4 and 8.0 eV, the sum of the present integral elastic and vibrational excitation cross sections are represented by (■).

The experimental DCS have been extrapolated and integrated at each energy in order to obtain the integral elastic cross section, which can be compared with the experimental total scattering cross sections obtained from attenuation measurements as well as with theory. These data are also presented in table 1 at the foot of each column of DCS data. The uncertainty in each value is estimated to be at least 25% as the process used for the extrapolation is somewhat arbitrary at some energies. Where possible the various theories have been used as a guide in the extrapolation process. However, at low energies and particularly at forward angles and in the region of the shape resonance, there are substantial differences between theory and experiment and the extrapolation has been done largely 'by eye'. The integral cross section data are compared with other measurements in figure 3. Given the good agreement between the present two sets of DCSs it is not surprising that the integral cross sections derived from them are also in good agreement. We also find very good agreement with the previous elastic scattering measurements of Johnstone and Newell (1993) and Marinkovic *et al* (1986). Also shown on this plot are the grand total cross section measurements of Kwan *et al* (1984) and Szmytkowski *et al* (1984). Of the three theoretical curves which are shown in this figure, the calculation of Winstead and McKoy best represents the overall energy dependence and magnitude of the total elastic scattering cross section. It also provides the best estimate of the position of the $^2\Pi$ shape resonance, being somewhat higher in energy than the *R*-matrix calculations (not shown).

In figure 4 we show the energy dependence of the elastic DCS in the region of the low-energy shape resonance at a number of scattering angles. The most notable aspect of this figure is the lack of any structure at an angle of 90°, whilst there is a strong broad resonance observed at both 30° and 130°. This is consistent with the classification of this resonance as

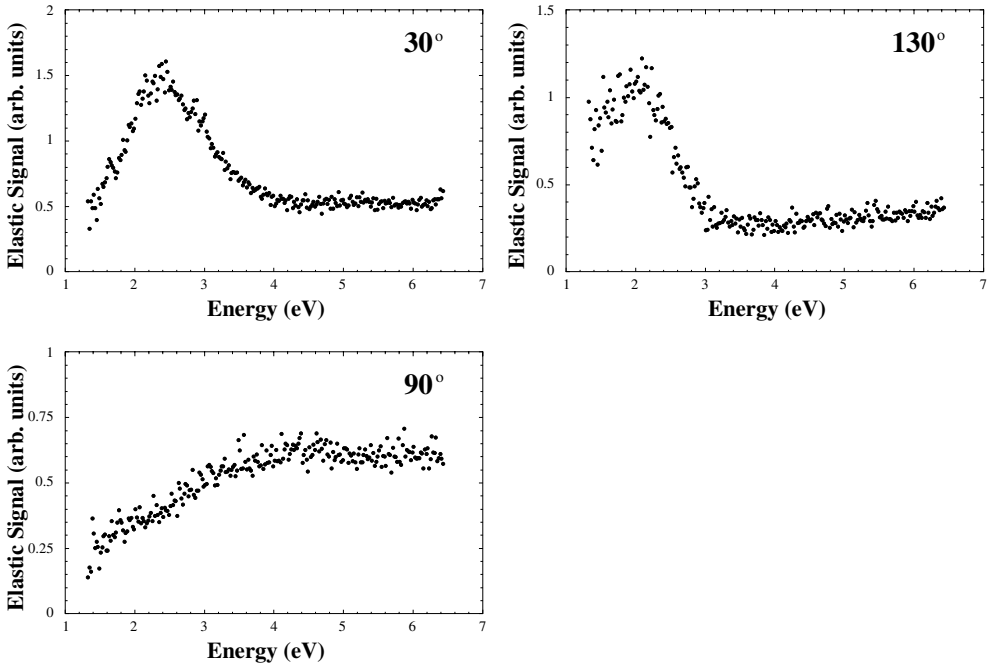

Figure 4. The energy dependence of the elastic DCS in the region of the $^2\Pi$ resonance at scattering angles of 30, 90 and 130°.

a $^2\Pi$ state which will decay into the elastic channel principally by the emission of a p-wave electron. The other interesting aspect shown in the figure is the apparent shift of the resonance peak at large scattering angles. The peak at 130° appears at an energy of about 2 eV and the structure is flatter on the low-energy side, whilst at 30° the peak position is about 2.2 eV and the cross section drops rapidly at lower energies. This may well be due to interference between the resonant and non-resonant (direct) scattering amplitudes.

3.2. Vibrational excitation

DCSs for the excitation of the first bending (010), symmetric stretch (100) and asymmetric stretch (001) vibrational modes have been measured at 2.4 and 8.0 eV. An example of an energy-loss spectrum, from which these cross sections were derived, is shown in figure 5. The tabulated values are presented in table 2 and the cross sections are shown in figures 6(*a*) and (*b*). These particular energies were chosen as they correspond to the positions of the two broad $^2\Pi$ and $^2\Sigma$ shape resonances, although the latter resonance is quite weak and has only been observed in vibrational excitation (Tronc *et al* 1981, Andric and Hall 1984).

At 2.4 eV (figure 6(*a*)) the excitation of the bending and symmetric stretch modes is quite strong and the symmetric stretch cross section shows strong p-wave character, indicting the contribution from the $^2\Pi$ resonance. The p-wave character is also evident in the DCS for the asymmetric stretch mode, although the cross section is considerably smaller than for the other two modes. This is also in contrast to the situation in CO_2 where almost no enhancement of the asymmetric stretch mode (100) was observed in the resonance region (e.g. Register *et al* 1980, Kitajima *et al* 2000). The DCS for the bending mode (010) shows a strong peak at around 100–120° and the cross section diminishes towards zero as the scattering angle approaches

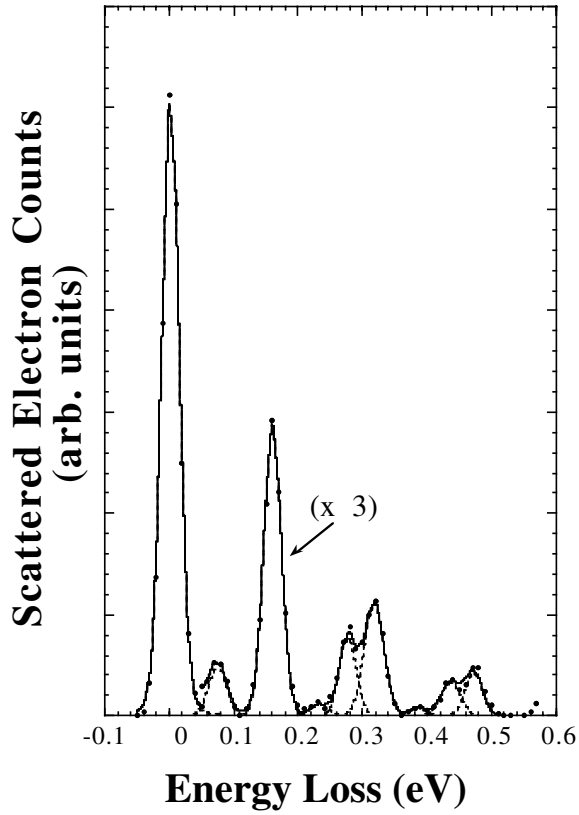

Figure 5. Energy-loss spectrum for N_2O at an incident energy of 2.4 eV and scattering angle of 30°. Also shown are the Gaussian functions arising from the fitting process. At energy-loss values greater than ∼50 meV, the data have been scaled by a factor of three.

0°. This overall trend is similar to that observed in the region of the $^2\Pi$ resonance in CO_2 and, in particular, the decrease of the bending mode DCS at small angles is consistent with the new resonant mechanism recently proposed by Cartwright and Trajmar (1996) for linear triatomic molecules. They note that there is no mechanism in the direct vibrational excitation in the ground state of these molecules to lead to such 'symmetry-forbidden' behaviour and they propose that it is a property of the intermediate negative-ion resonance. In their model the symmetry-forbidden signature arises from autodetachment from a bent CO_2^- resonant state, which has been formed by electron attachment to electronically excited, bent CO_2 neutral molecules, and which has negative reflection symmetry in the plane of the molecule. Thus their model is fundamentally different from the 'boomerang' model which pictures this resonance, and the corresponding feature in N_2O, as a shape resonance associated with the (linear) ground state of the molecule.

At 8.0 eV (figure 6(*b*)) all the vibrational excitation cross sections are smaller than the above by about a factor of five or more. The DCS for the symmetric stretch mode (100) shows a combination of both p- and d-wave character and is the strongest of the three vibrational excitations. The angular behaviour of the (010) mode is similar to that observed at 2.4 eV, although this conclusion is a little tentative as the scatter in the data at this energy is much larger than at 2.4 eV. For the (001) mode almost the same angular dependence is seen as for

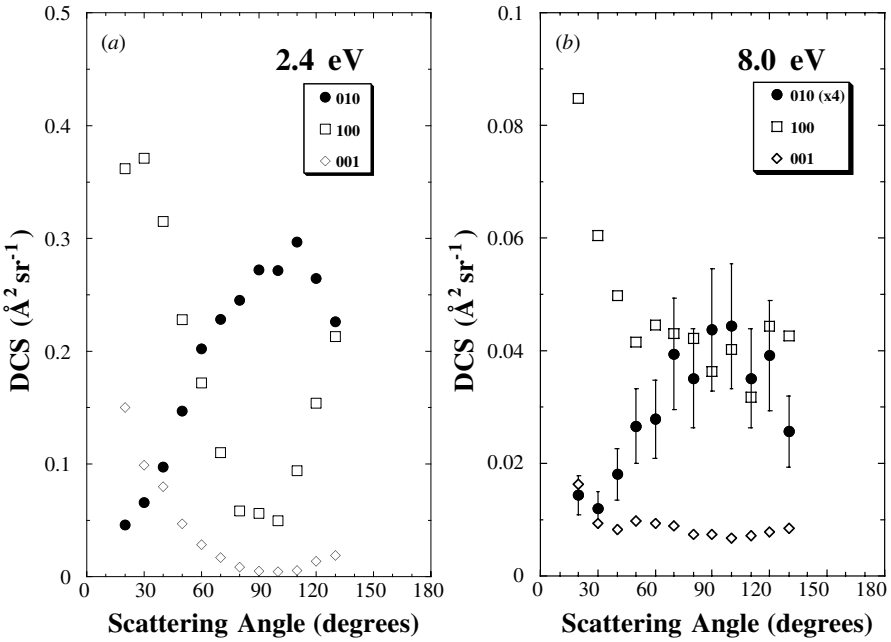

Figure 6. (*a*) DCS for vibrational excitation of N_2O at 2.4 eV. (●) Bending mode (010); (□) symmetric stretch (100); (◇) asymmetric stretch (001). (*b*) DCS for vibrational excitation of N_2O at 8.0 eV. (●) Bending mode (010); (□) symmetric stretch (100); (◇) asymmetric stretch (001). Note that the bending mode cross section has been scaled by a factor of four. The error bars in this case are estimates of the 'shape' uncertainty in the cross section (∼25%). Absolute uncertainties are given in table 2.

the (100) excitation. Andric and Hall (1984) have shown that this angular dependence in their relative DCS is well described by the angular correlation theory of Read (1968) assuming excitation via a Σ resonance. This is also the case for the present results although comparison with *ab initio* theoretical cross sections for vibrational excitation would be advantageous in this region.

The vibrational DCSs have been extrapolated and integrated, using the angular correlation theory as a guide, to obtain integral vibrational excitation cross sections at 2.4 and 8.0 eV. These values are shown at the foot of each column in table 2. The uncertainties in these cross sections are estimated to be between 30% and 50%, depending on the vibrational level and the scattering angle. At low energies one might expect that the sum of the present rotationally summed integral elastic cross section plus the rotationally summed integral vibrational excitation cross sections should be similar to the grand total cross sections in the resonance region. We see from figure 3 that this is clearly not the case and, at an energy of 2.4 eV, the combined integral cross sections from the present data (18.9 $Å^2$) are substantially lower than either of the two grand total cross sections (∼28 $Å^2$). One can only speculate as to the cause of this discrepancy. The present analysis does not include vibrational harmonics but these are unlikely to account for the observed differences. The differences may highlight the inadequacies of the arbitrary extrapolation techniques which have, by necessity, been used to obtain the integral elastic cross sections from differential scattering data.

Table 2. Absolute cross sections for vibrational excitation of N_2O at 2.4 eV and 8.0 eV (in units of 10^{-16} cm^2 sr^{-1}). The estimated percentage uncertainties in the DCS are shown at the foot of each column. Q_i is the integral vibrational cross section (in units of 10^{-16} cm^2).

	Energy (eV)					
	2.4 eV			8.0 eV		
Angle (deg)	010	100	001	010	100	001
20	0.046	0.362	0.15	0.0036	0.0850	0.0162
30	0.066	0.371	0.099	0.0030	0.0605	0.0092
40	0.097	0.315	0.08	0.0045	0.0498	0.0083
50	0.147	0.228	0.047	0.0066	0.0416	0.0096
60	0.202	0.172	0.029	0.0070	0.0445	0.0093
70	0.228	0.11	0.017	0.0099	0.0431	0.0088
80	0.245	0.058	0.009	0.0088	0.0422	0.0074
90	0.272	0.056	0.005	0.0109	0.0363	0.0073
100	0.311	0.065	0.003	0.0111	0.0402	0.0067
110	0.297	0.094	0.005	0.0088	0.0317	0.0071
120	0.264	0.154	0.011	0.0098	0.0443	0.0077
130	0.226	0.213	0.019	0.0064	0.0425	0.0084
	30%	30%	50%	50%	30%	50%
Q_i	2.67	2.92	0.45	0.11	0.74	0.14

4. Conclusions

The present work provides a comprehensive set of data for elastic scattering and vibrational excitation of N_2O at low to intermediate energies. It also demonstrates a high level of accord between the experimental measurements from our two laboratories that have been gathered on two separate electron spectrometers with many similarities but, notably, also many differences. This provides us with confidence that, when there is careful attention to the detailed application of the relative flow technique, accurate absolute cross sections can be obtained.

We have discussed the behaviour of the elastic DCS at small scattering angles and low incident energies for several other molecules on previous occasions (e.g. Buckman *et al* 1998, Gibson *et al* 1999). The observation of the minimum in the cross section at small scattering angles for N_2O, the rapid energy dependence of the development of this feature, and the narrow energy range over which it exists, provide further compelling evidence that this behaviour is common to many molecules. We have now observed it in a number of systems (e.g. N_2, NO, O_2, CO, CO_2, NF_3, C_6H_6) with a wide variety of molecular structures (closed shell, open shell, diatomic, polyatomic, non-polar and mildly polar). In each case the structure develops above the low-lying (1–4 eV) shape resonances which are common to these molecules and it has largely disappeared by the time the energy has reached 10 eV. One other common feature in all of these molecules is the failure of contemporary scattering theory to reproduce this structure. Indeed, for the present measurements of elastic scattering there is rather poor accord between theory and experiment with the possible exception of the energy region of the $^2\Pi$ resonance and for energies in excess of 10 eV. Unfortunately, this situation is also observed in many other polyatomic molecules and indicates the level of complexity that low-energy electron–molecule interactions pose, even for state-of-the-art scattering calculations. Of the various theoretical approaches that have been employed, it is difficult to discriminate between their effectiveness at energies below 10 eV. It is possible that the *R*-matrix calculation of

Morgan *et al* shows a slightly better level of agreement with the experiments when it comes to the description of the subtleties of the angular distributions. At energies of 10 eV and above there is little difference between the various calculations and, in general, the agreement between experiment and theory is quite good. This is consistent with the observation by Winstead and McKoy (1998) that, for instance, there is little difference between the static exchange and static exchange + polarization calculations at these energies.

The present results for vibrational excitation show broadly similar behaviour in the region of the $^2\Pi$ resonance to that which has been observed in CO_2. The 'symmetry-forbidden' nature of the DCS for the (010) vibrational excitation mode as predicted by the model of Cartwright and Trajmar (1996) is clearly evident at the energy of the $^2\Pi$ resonance. There is further evidence that similar behaviour is seen for the 8 eV resonance, although the quality of the data is not as high at this energy. Further studies of these, and higher bending overtones, require substantially higher energy resolution and better statistics but would nonetheless be worthwhile. Detailed interpretation of these cross sections would also benefit greatly from *ab initio* theoretical input.

Acknowledgments

SJB wishes to thank the Japan Society for the Promotion of Science for the provision of a short-term Visiting Fellowship and Professor Hiroshi Tanaka and his colleagues for their hospitality during a visit to Sophia University, where this manuscript was prepared. We are indebted to Professor Mineo Kimura for his comments on the manuscript. RJG thanks the Australian Research Council for the provision of a Postdoctoral Fellowship and JG thanks the Australian National University for the provision of a Graduate School Scholarship. We also acknowledge some very helpful comments from two referees on the initial version of this manuscript.

References

Andric L and Hall R I 1984 *J. Phys. B: At. Mol. Phys.* **17** 2713
Boesten L and Tanaka H 1992 *At. Data Nucl. Data Tables* **52** 25
Brunt J N H, King G C and Read F H 1977 *J. Phys. B: At. Mol. Phys.* **10** 1289
Buckman S J, Gibson J C and Brunger M J 1998 *Photonic, Electronic and Atomic Collisions* ed F Aumayr and H Winter (Singapore: World Scientific)
Buckman S J, Gulley R J and Brunger M J 1994 *Electron Collisions with Molecules, Clusters and Surfaces* vol 1, ed H Ehrhardt and L A Morgan (New York: Plenum)
Buckman S J, Gulley R J, Moghbelalhossein M and Bennett S 1993 *Meas. Sci. Technol.* **4** 1143
Cartwright D C and Trajmar S 1996 *J. Phys. B: At. Mol. Opt. Phys.* **29** 1549
da Costa S M S and Bettega M H F 1998 *Eur. Phys. J.* D **3** 67
Dillon M A, Boesten H, Tanaka H, Kimura M and Sato H 1993 *J. Phys. B: At. Mol. Opt. Phys.* **26** 3147
Fursa D V and Bray I 1995 *Phys. Rev.* A **52** 1279
Gibson J C, Green M A, Trantham K W, Buckman S J, Teubner P J O and Brunger M J 1999 *J. Phys. B: At. Mol. Opt. Phys.* **32** 213
Gulley R J, Alle D T, Brennan M J, Brunger M J and Buckman S J 1994 *J. Phys. B: At. Mol. Opt. Phys.* **27** 2593
Johnstone W M and Newell W R 1993 *J. Phys. B: At. Mol. Opt. Phys.* **26** 129
Kitajima M, Sakomoto Y, Watanabe S, Suzuki T, Ishikawa T, Tanaka H and Kimura M 1999 *Chem. Phys. Lett.* **309** 414
Kitajima M, Watanabe S, Tanaka H, Takekawa M, Kimura M and Itikawa Y 2000 *Phys. Rev.* at press
Kubo M, Matsunaga D, Suzuki T and Tanaka H 1981 *Proc. 12th ICPEAC: Int. Conf. on Physics of Electronic and Atomic Collisions (Gatlinburg)* ed S Datz *et al* (Amsterdam: North-Holland) p 360
Kwan Ch K, Hsieh Y-F, Kauppila W E, Smith S J, Stein T S and Uddin M N 1984 *Phys. Rev. Lett.* **52** 1417
Marinkovic B, Szmytkowski Cz, Pejcev V, Filipovic D and Vuskovic L 1986 *J. Phys. B: At. Mol. Phys.* **19** 2365
Michelin S E, Kroin T and Lee M T 1996 *J. Phys. B: At. Mol. Opt. Phys.* **29** 2115
Morgan L A, Gillan C J, Tennyson J and Chen X 1997 *J. Phys. B: At. Mol. Opt. Phys.* **30** 4087

Nesbet R K 1979 *Phys. Rev.* A **20** 58
Nickel J C, Zetner P W, Shen G and Trajmar S 1989 *J. Phys. E: Sci. Instrum.* **22** 730
Read F H 1968 *J. Phys. B: At. Mol. Phys.* **1** 893
Register D F, Nishimura H and Trajmar S 1980 *J. Phys. B: At. Mol. Phys.* **13** 1651
Rohr K 1977 *J. Phys. B: At. Mol. Phys.* **10** 2215
Sagara T and Boesten L 1998 *J. Phys. B: At. Mol. Opt. Phys.* **31** 3455
Sarpal B K, Pfingst K, Nestmann B M and Peyerimhoff S D 1996 *J. Phys. B: At. Mol. Opt. Phys.* **29** 857
Shi X, Stephen T M and Burrow P D 1993 *J. Phys. B: At. Mol. Opt. Phys.* **26** 121
Srivastava S K, Chutjian A and Trajmar S 1975 *J. Phys. Chem.* **63** 2659
Szmytkowski Cz, Karwasz G and Maciag K 1984 *Chem. Phys. Lett.* **107** 481
Tanaka H, Boesten L, Matsunaga D and Kudo T 1988 *J. Phys. B: At. Mol. Opt. Phys.* **21** 1255
Tronc M, Malegat L, Azria R and Le Coat Y 1981 *Proc. 12th ICPEAC: Int. Conf. on Physics of Electronic and Atomic Collisions (Gatlinburg)* ed S Datz (Amsterdam: North-Holland) p 372
Winstead C and McKoy V 1998 *Phys. Rev.* A **57** 3589
Zecca A, Lazzizzera I, Krauss M and Kuyatt C E 1974 *J. Phys. Chem.* **61** 4560